# Semisynthesis of Fluorescent Metabolite Sensors on Cell Surfaces

Matthias A. Brun, Rudolf Griss, Luc Reymond, Kui-Thong Tan,[†] Joachim Piguet, Ruud J.R.W. Peters,[‡] Horst Vogel, and Kai Johnsson*

Institute of Chemical Sciences and Engineering, Institute of Bioengineering, National Centre of Competence in Research Chemical Biology, École Polytechnique Fédérale de Lausanne, Lausanne, Switzerland.

S *Supporting Information*

ABSTRACT: Progress in understanding signal transduction and metabolic pathways is hampered by a shortage of suitable sensors for tracking metabolites, second messengers, and neurotransmitters in living cells. Here we introduce a class of rationally designed semisynthetic fluorescent sensor proteins, called Snifits, for measuring metabolite concentrations on the cell surface of mammalian cells. Functional Snifits are assembled on living cells through two selective chemical labeling reactions of a genetically encoded protein scaffold. Our best Snifit displayed fluorescence intensity ratio changes on living cells significantly higher than any previously reported cell-surface-targeted fluorescent sensor protein. This work establishes a generally applicable and rational strategy for the generation of cell-surface-targeted fluorescent sensor proteins for metabolites of interest.
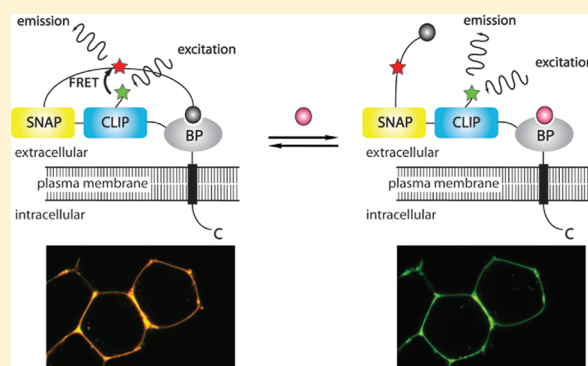
■ INTRODUCTION

It is estimated that the primary and secondary metabolism of an animal cell comprises about 7900 metabolites.[1] Furthermore, the concentration of these metabolites can fluctuate. For example, the concentration of neurotransmitters can change within milliseconds by orders of magnitude, and the concentration of the central cofactor nicotinamide adenine dinucleotide (NAD^+) has been shown to oscillate with the same frequency as the circadian rhythm.[2] Additionally, these concentration changes are generally confined to certain compartments within the cell. Notably, the extracellular cell surface represents an extremely dynamic microenvironment of the cell, as concentration transients of neurotransmitters and hormones on the cell surface of neurons and other specialized cell types regulate important cellular processes such as chemical neurotransmission. Undoubtedly, the determination of the concentration of metabolites with both high spatial and temporal resolution is a prerequisite for an in-depth understanding of various biological processes.

Fluorescent-based sensors are an attractive approach for noninvasive sensing of metabolites in living cells.[3] While fluorescent sensors for various metabolites exist, many of these sensors are not suitable for measuring metabolite concentrations in cells with high temporal and spatial resolution.[4,5] Currently, the majority of sensors used for measuring metabolite concentrations in living cells are biosensors based on Förster resonance energy transfer (FRET).[3,6] The design of FRET-based biosensors for metabolites is usually based on a protein that undergoes a conformational change upon binding of the analyte of interest. Sandwiching such a protein between two autofluorescent proteins (FP) can then result in the generation of a FRET-based

biosensor.[7,8] Although biosensors for various metabolites have been developed,[9–12] for most metabolites of interest no sensors exist and in particular for applications on cell surfaces very few biosensors have been reported.[10,12] There are different reasons for the scarcity of FRET-based biosensors for metabolites: First, only binding proteins that undergo a conformational change upon ligand binding can be used for the generation of such biosensors[13] and for many metabolites no such binding proteins are available. Second, biosensors for metabolites often display relatively small maximum ratio changes.[14] When targeted to the cell surface, fluorescent sensor proteins retained in the secretory pathway result in background signal that further decreases the maximum ratio change. Therefore, the construction of suitable FP-based biosensors often requires the optimization of their maximum ratio change.[10] This mostly involves time-consuming random screening of sensor protein libraries and this process has to be repeated for each new biosensor.

The challenges associated with generating FRET-based biosensors call for alternative strategies for the generation of fluorescent sensors suitable for applications in cells. Here we introduce a new class of sensor proteins, called Snifits (**S**NAP-tag based **i**ndicator proteins with a **f**luorescent **i**ntramolecular **t**ether), for visualizing the concentration of metabolites on the cell surface of mammalian cells. The approach builds on our previously reported strategy to generate FRET-based sensor proteins for metabolites that circumvents the obligatory conformational change of a binding protein.[15] For the application of our Snifit sensor concept on
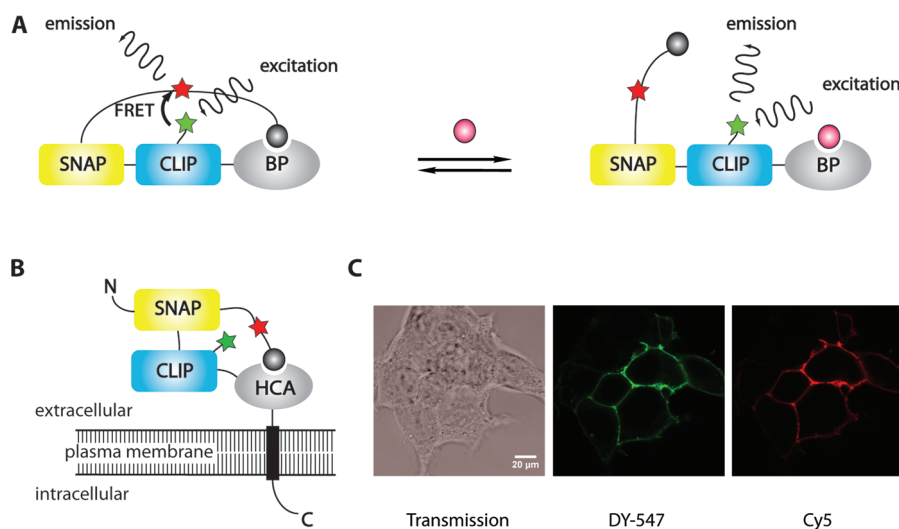
Figure 1. Design principle and expression of the semisynthetic sensor proteins on the surface of HEK 293T cells. (A) Semisynthetic sensor proteins. The protein part of the sensor is a fusion protein of SNAP-tag, CLIP-tag, and a binding protein (BP). The active semisynthetic sensor protein is obtained by labeling SNAP-tag with a molecule containing a fluorophore (red star) and a ligand for the binding protein (gray ball) and by labeling CLIP-tag with a second fluorophore (green star). In the absence of analyte (pink ball), the intramolecular ligand binds to the binding protein, keeping the sensor protein in a closed conformation. Donor and acceptor fluorophores are in close proximity, resulting in a high FRET efficiency. In the presence of analyte, the intramolecular ligand is displaced, and the sensor protein shifts toward an open conformation. Donor and acceptor fluorophore are more distant from each other than in the closed conformation and FRET efficiency therefore decreases. (B) Design of the sensor protein on the cell surface. SNAP_CLIP_HCA was fused to a transmembrane domain (truncated PDGF receptor, pDisplay) for its display on the extracellular surface of mammalian cells. (C) SNAP_CLIP_HCA was labeled on the cell surface of HEK 293T cells with the dyes DY-547 and DY-647 via their corresponding O^2-benzylcytosine (BC)- and O^6-benzylguanine (BG)-derivatives. Images were taken using a confocal Zeiss LSM 700 microscope.

cell surfaces, we demonstrate that the protein part of the sensor can be genetically encoded and the functional Snifit is generated on the surface of live mammalian cells through two specific labeling reactions. The use of Snifits on living cells represents an important advance in the development of this sensor family. Furthermore, the rational design of Snifits permits the use of simple optimization guidelines to improve the performance of the sensor. The work described here therefore establishes a rational strategy for the generation of cell-surface based fluorescent sensors.

RESULTS AND DISCUSSIONS

Snifit Sensor Proteins on the Cell Surface of Mammalian Cells. The Snifit sensor protein concept employs a covalently attached synthetic fluorescent ligand to distinguish between the presence and the absence of analyte. The sensor protein is functionalized with the synthetic ligand using the SNAP-tag labeling technology.[16] In the absence of analyte, the sensor protein is in the closed conformation, in which the synthetic ligand binds to the binding protein in an intramolecular fashion; the presence of analyte displaces the intramolecular ligand from the binding protein and thereby shifts the sensor protein to an open conformation (Figure 1A). This competitive displacement of the intramolecular ligand by free analyte can be detected by a change in the FRET efficiency of the sensor protein.[15] In order to study the applicability and general properties of our Snifit sensor proteins on the cell surface, we set out to construct a cell surface targeted version of our proof-of-concept Snifit sensor protein using human carbonic anhydrase II (HCA) as the binding protein (Figure 1B). In the first part of our work we describe the design and full characterization of the cell-surface bound sensor. This involves the optimization of its cell-surface expression level, the response of the sensor at the cell surface, its

metabolite affinity, and sensing kinetics. We further demonstrate the versatility with regard to fluorescent dyes and investigate whether the sensor kinetics can be tuned according to individual requirements. In the second part, we perform a successful optimization of our model Snifit sensor protein in vitro and on the cell surface by the rational design of its peptide linkers. While there are no immediate applications for a Snifit with HCA as binding protein, this work establishes the necessary foundation for applying our concept to other metabolites.

The sensor protein SNAP_CLIP_HCA was successfully expressed as a fusion to a transmembrane anchor on the surface of HEK 293T cells, as demonstrated by labeling SNAP- and CLIP-tag with the two synthetic dyes DY-647 and DY-547, respectively (Figure 1C). The synthetic precursor for the assembly of the semisynthetic sensor protein on the cell surface follows the same design guidelines as in our previous work.[15] It contains a O^6-benzylguanine (BG) moiety for reaction with SNAP-tag, an 11-PEG-unit linker, a Cy5 fluorophore which is an integral part of the linker, and a terminal para-benzenesulfonamide moiety. However, we exchanged the nonsulfonated Cy5 fluorophore by a Cy5 derivative that contains two sulfonate groups (BG-PEG$_{11}$-Cy5-paraSA **1**, Figure 2A) to render the BG substrate less hydrophobic and therefore better suitable for specific labeling of cell surface proteins. In parallel, we synthesized a BG derivative that contains a terminal meta-benzenesulfonamide instead of the para-benzenesulfonamide (BG-PEG$_{11}$-Cy5-metaSA **2**). Further, we also synthesized derivatives of Alexa Fluor 488 (BG-PEG$_{11}$-Alexa Fluor 488-SA **4**), and of Alexa Fluor 594 (BG-PEG$_{11}$-Alexa Fluor 594-SA **5**), for the creation of alternative FRET pairs (Figure 2B,C). For control experiments we synthesized BG-PEG$_{11}$-Cy5 **3**, BG-PEG$_{11}$-Alexa Fluor 488 **6**, and BG-PEG$_{11}$-Alexa Fluor 594 **7** lacking the terminal benzenesulfonamide moiety (Figure 2A−C).

A

1 R = HN (PEG) 2 NH —benzenesulfonamide (para)

2 R = HN (PEG) 2 NH —benzenesulfonamide (meta)

3 R = OH

B

4 R = HN (PEG) 2 NH —SA

6 R = NH₂
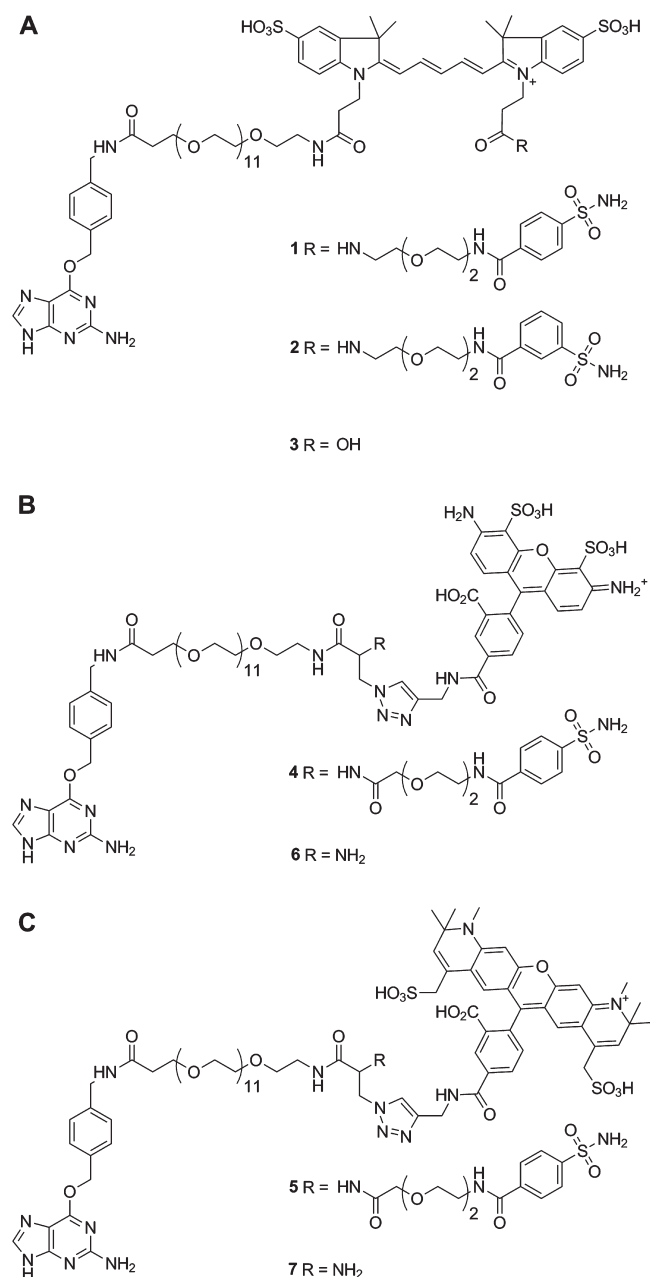
C

5 R = HN (PEG) 2 NH —SA

7 R = NH₂

Figure 2. Substrates for SNAP-tag sensor protein labeling. (A) BG-PEG₁₁-Cy5-paraSA **1**. BG-PEG₁₁-Cy5-metaSA **2**. (B) BG-PEG₁₁-Alexa Fluor 488-SA **4**. (C) BG-PEG₁₁-Alexa Fluor 594-SA **5**. The molecules **3**, **6**, and **7** are the corresponding control molecules lacking the terminal benzenesulfonamide moiety.

To assemble the sensor at the extracellular surface of mammalian cells, we labeled HEK 293T cells expressing SNAP_CLIP_HCA on the cell surface with BG-PEG₁₁-Cy5-SA **1** (2 μM) and CLIP-Surface 547 (10 μM) for 10 min at RT (Figure 3A). CLIP-Surface 547 is a substrate for labeling CLIP-tag with the fluorescent dye DY-547. To determine the response of the sensor at the cell surface to added inhibitor, we applied a solution of 10 mM benzenesulfona-mide in HBSS to the HEK 293T cells by using a perfusion system, and monitored the intensity ratio of DY-547/Cy5 fluorescence by microscopy. We found a sulfonamide-dependent DY-547/Cy5 ΔR_{max} of 1.5 ± 0.1 that was fully reversible upon perfusion of the HEK 293T cells with HBSS without inhibitor (Figure 3C). In order

to verify that the observed ratio change is indeed due to a specific displacement of the intramolecular ligand from the active site of HCA, we labeled HEK 293T cells expressing SNAP_CLIP_HCA on the cell surface with BG-PEG₁₁-Cy5 **3**, a molecule lacking the terminal para-benzenesulfonamide moiety (Figure 2A), and with CLIP-Surface 547. Perfusion of this control sensor with 10 mM benzenesulfonamide did not induce any intensity ratio change of DY-547/Cy5 (Figure S1).

Determination of the K_d^{comp} of the Sensor Protein. It is critical for the performance of the sensor that the physiological concentration of the analyte of interest matches the affinity of the sensor protein for its analyte. The binding isotherm of our sensor protein reflects a competition between the free inhibitor and the intramolecularly bound inhibitor.[15] Thus, the binding curve is characterized by a dissociation constant for the free ligand ($K_d^{comp,ligand}$), which equals the amount of free ligand that needs to be added to displace the intramolecular ligand in 50% of the sensors. We first determined the $K_d^{comp,SA}$ for the sensor on the cell surface of HEK 293T cells by perfusion with increasing concentrations of benzenesulfonamide and found a value of $K_d^{comp,SA}$ = 600 ± 250 μM (Figure 4A,B). The here measured $K_d^{comp,SA}$ is in agreement with the $K_d^{comp,SA}$ found for soluble sensor (340 ± 60 μM),[15] and indicates that the sensor protein retains its properties when displayed on the cell surface. We then also determined the K_d^{comp} for cells expressing the sensor protein at low, medium, and high densities to investigate if sensor proteins interact in an intermolecular fashion at high local sensor protein concentrations. In the latter case, the measured K_d^{comp} would become dependent on the concentration of the sensor protein. We found that the $K_d^{comp,SA}$ did not significantly change for different cells expressing the sensor protein at varying concentrations on the cell surface (Supporting Information), indicating that the binding of the attached ligand is indeed predominantly intramolecular even at higher local sensor protein concentrations.

Variety of Synthetic Fluorophores Can Be Applied for Sensor Construction. Synthetic fluorophores provide spectro-scopic properties, such as high photostability or infrared excita-tion and emission maxima, which cannot be found in any of the currently existing FPs.[17,18] Since the use of self-labeling tags permits the inclusion of any synthetic fluorophore into the sensor proteins, we wanted to demonstrate the versatility of the sensor concept in terms of the employed fluorophore pair for FRET. For this purpose, we labeled our sensor protein on the cell surface with two different fluorophore pairs, Alexa Fluor 488/DY-547 and Alexa Fluor 488/Alexa Fluor 594. Both combinations showed benzenesulfonamide-dependent donor/acceptor inten-sity ratio changes. We found a ΔR_{max} of 1.3 ± 0.1 for the combination Alexa Fluor 488/DY-547 (Figure S2) and a ΔR_{max} of 1.7 ± 0.1 for the Alexa Fluor 488/Alexa Fluor 594 FRET pair (Figure S3). Control experiments with the corresponding BG substrates lacking the terminal benzenesulfonamide moiety again did not exhibit any donor/acceptor intensity ratio change, demonstrating that the response of the biosensor is due to a specific interaction between HCA and the intramolecular ligand (Figures S4, S5).

The use of two synthetic dyes for the construction of cell surface biosensors avoids another problem of FP-based biosen-sors. By employing membrane-impermeable dyes, only sensor proteins that are properly trafficked to the cell surface are labeled. To illustrate this, we constructed a cell surface-targeted version of the sensor protein SNAP_mCherry_HCA, in which CLIP-tag is
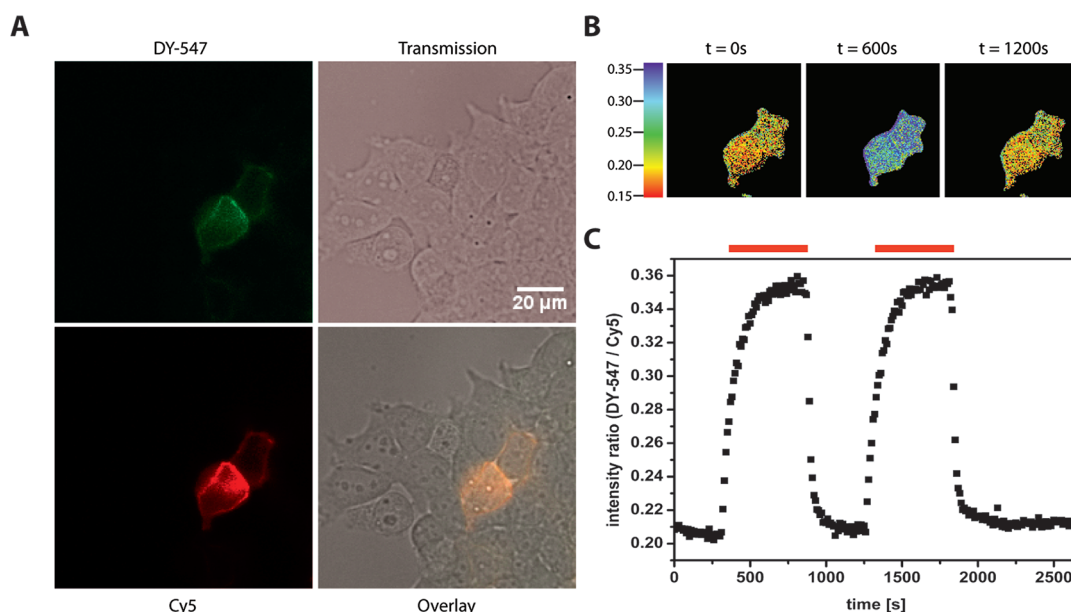
Figure 3. SNAP_CLIP_HCA as a sensor for sulfonamides on the surface of HEK 293T cells. (A) Donor channel (DY-547), FRET channel (Cy5), and transmission channel of the labeled sensor protein on HEK 293T cells. Images were taken using a Leica LAS AF 7000 wide-field microscope. (B) Ratio images of the labeled sensor protein in absence of free benzenesulfonamide ($t = 0$ s, $t = 1200$ s) and in the presence of 10 mM free benzenesulfonamide ($t = 600$ s). (C) Time course of sensor opening (upon addition of 10 mM benzenesulfonamide) and of sensor closing (upon removal of the free benzenesulfonamide). The red bar indicates the time span of perfusion with benzenesulfonamide.

replaced by the red FP mCherry (Figure S6A). SNAP_mCherry_HCA and SNAP_CLIP_HCA perform very similarly as purified sensors in vitro.[15] As expected, SNAP_mCherry_HCA can also be labeled on the cell surface via SNAP-tag. However, it also exhibits a strong fluorescent signal in the secretory pathway due to the inherent fluorescence of mCherry (Figure S6B). Evidently, this intracellular background fluorescence makes the analysis of the FRET sensors on the cell surface more demanding, especially in cases where the location of the sensor protein cannot clearly be resolved by confocal microscopy, such as for the analysis of cells in living tissue or for high-throughput screening applications in microtiterplates.

Kinetic Characterization of the Sensor Proteins. The temporal resolution of our sensor proteins is determined by the rate of sensor opening and sensor closing. Ideally, these rates should exceed the rate of the small molecule's concentration change. The kinetic requirements of the sensor protein heavily depend on the type of molecule; e.g., the concentration change of most hormones takes places within minutes. On the other hand, neurotransmitter release and clearance occurs on a millisecond time scale. For our sensor protein, sensor opening and sensor closing are composed of two separate steps, i.e., the unbinding of the intramolecular ligand followed by the binding of the free ligand for sensor opening, and the unbinding of the free ligand followed by the binding of the intramolecular ligand for sensor closing (Figure S7). As the temporal resolution of a biosensor is important for biological applications, we wanted to characterize the kinetics mechanisms of opening and closing of our sensor protein. For that purpose, we measured the rates of sensor opening and closing for our sensor protein upon addition and removal of benzenesulfonamide and then also for two additional inhibitors of HCA, i.e., methazolamide, and ethoxzolamide. All three inhibitors possess significantly different k_{on} and k_{off} values (Table S1)[19] and should therefore also generate different opening

and closing rates of the sensor protein. HEK 293T cells expressing the sensor protein were consecutively perfused with 10 mM benzenesulfonamide, 1 mM methazolamide, and 10 μM ethoxzolamide (Figure 4C). All concentrations were chosen to set the sensor protein at saturating (open state) conditions. For the perfusion with 10 mM benzenesulfonamide, we found best-fit parameters of $t_{1/2,open} = 60 \pm 5$ s for sensor opening and of $t_{1/2,close} = 40 \pm 10$ s for sensor closing by fitting the DY-547/Cy5 ratio time course to a single exponential function (Figure S8). Analogously, we measured $t_{1/2,open} = 65 \pm 5$ s and $t_{1/2,close} = 65 \pm 15$ s for the perfusion with 1 mM methazolamide, and $t_{1/2,open} = 80 \pm 15$ s and $t_{1/2,close} = 150 \pm 15$ s for the perfusion with 10 μM ethoxzolamide. The $t_{1/2,close}$ value for ethoxzolamide was significantly larger than the $t_{1/2,close}$ value for benzenesulfonamide. This is in agreement with its slower k_{off} values compared to benzenesulfonamide (Tables S1, S2) and suggests that the rate of sensor closing mainly depends on the unbinding of the free ligand and not on the (re)binding of the intramolecular ligand because the latter step is the same for all three inhibitors. In contrast, we found that the $t_{1/2,open}$ value for sensor opening did not change significantly for the three inhibitors. This indicates that the rate of sensor opening mainly depends on the unbinding of the intramolecular ligand. In agreement with this hypothesis, we found that by changing the intramolecular para-substituted benzenesulfonamide to a meta-substituted benzenesulfonamide, which exhibits a faster k_{off} value toward HCA,[19] the sensor opens about 10 times faster upon perfusion with 500 μM benzenesulfonamide ($t_{1/2,open} = 7 \pm 2$ s) (Figure 4D, Figures S9, S10). The $t_{1/2,close}$ for sensor closing does not change significantly compared to the para-substituted benzenesulfonamide ($t_{1/2,close} = 25 \pm 5$ s) and confirms that the rate of sensor closing mainly depends on the unbinding of the free ligand. These experiments demonstrate how it is possible to tune the kinetics of sensor opening by choosing an appropriate intramolecular ligand. The rate of sensor closing
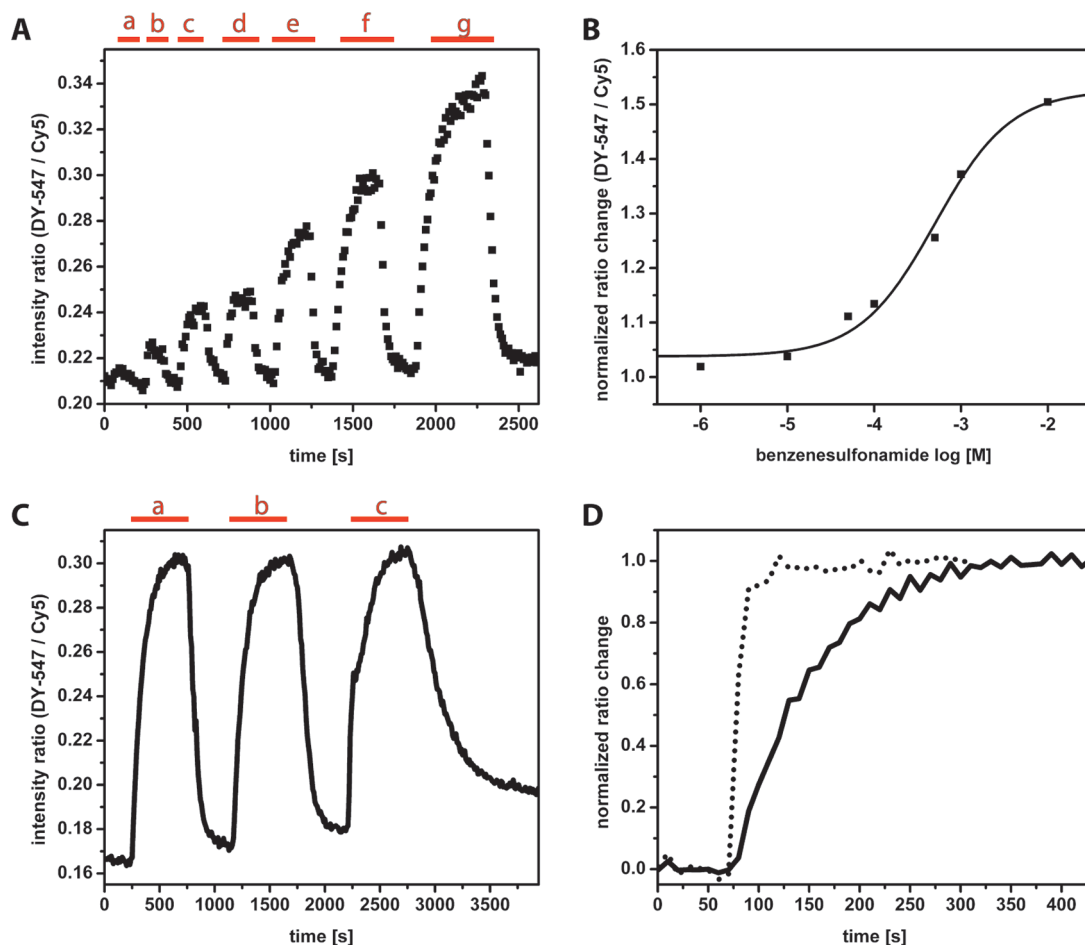
Figure 4. Kinetic and thermodynamic characterization of the sensor protein SNAP_CLIP_HCA on the surface of HEK 293T cells. (A) Time course of perfusion of labeled SNAP_CLIP_HCA with increasing concentrations of benzenesulfonamide ($a = 1\,\mu M$, $b = 10\,\mu M$, $c = 50\,\mu M$, $d = 100\,\mu M$, $e = 500\,\mu M$, $f = 1$ mM, $g = 10$ mM). (B) Benzenesulfonamide titration curve of SNAP_CLIP_HCA on the extracellular surface of HEK 293T cells. (C) Time course of sensor opening and closing upon perfusion with 10 mM benzenesulfonamide (a), with 1 mM methazolamide (b), and with 10 μM ethoxzolamide (c). (D) Comparison of the opening rate between a sensor protein labeled with the terminal para-benzenesulfonamide (solid line) and a sensor protein labeled with the terminal meta-benzenesulfonamide (dotted line) upon addition of 10 mM benzenesulfonamide.

mainly depends on the unbinding of the analyte and is therefore a characteristic of the binding protein.

Rational Optimization of the Semisynthetic Sensor Protein Scaffold. After having demonstrated the successful implementation of our Snifit sensor proteins on the cell surface, we set out to investigate whether it is possible to optimize the sensor protein scaffold regarding the dynamic range of its signal change. The maximum ratio change of a FRET-based sensor is one of the key parameters for its efficient application in a cellular setting or in a whole organism. It determines whether the sensor exhibits a sufficient signal over noise and can thus be used to measure a reliable signal of the sensor response. Although there is no clear threshold above which the dynamic range of a certain FRET sensor is said to be sufficiently high, it is generally acknowledged that the higher the dynamic range of a sensor is, the more reliably its signal can be interpreted.[20] Since the majority of FRET sensors based on FPs still suffer from a rather small dynamic range, the optimization of FRET sensors in terms of their dynamic range is an area of active research.[20] Strategies for the optimization of FRET sensors include the use of improved fluorescent proteins,[21] different FRET pairs,[22] and the mutations of the peptide linkers between the protein units

of the FRET sensor[10,23] in combination with a suitable screening technique to analyze sensor mutant libraries. However, while there are an impressive number of successful examples for the optimization of FRET-based sensors, there is still no general way that allows the design and improvement of a FRET sensor in a rational way.

The key to rationally optimize a FRET sensor is to understand and exploit its molecular mechanism. On the basis of our sensor model we hypothesized that shortening the linker between CLIP-tag and HCA would increase FRET efficiency in the closed state while increasing the linker length between SNAP-tag and CLIP-tag should decrease FRET efficiency in the open state.[15] In both cases the result should be an increase of the performance of the sensor protein. Our original sensor protein SNAP_CLIP_HCA contains a flexible linker of 18 amino acids between SNAP-tag and CLIP-tag and a flexible linker of six amino acids between CLIP-tag and HCA, respectively. Despite their frequent use, flexible peptide linkers are not a very efficient means to gain distance between two proteins because these linkers can occupy a wide range of conformations in space.[23,24] Therefore, we pursued a different strategy to alter the effective linker length. Poly-L-proline linkers have been used for a long time as precise molecular rulers due to
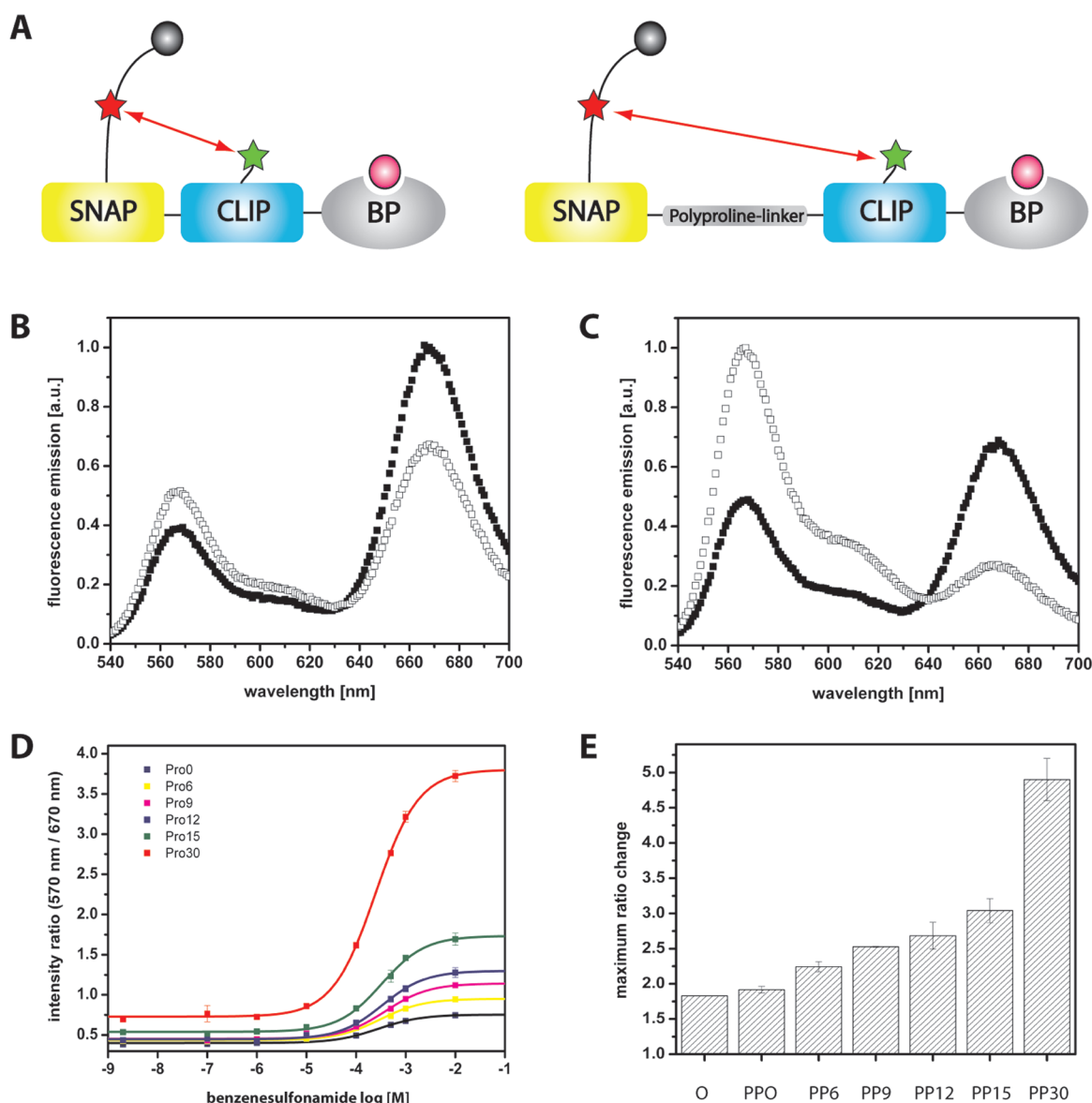
Figure 5. Rational optimization of the semisynthetic sensor protein for sulfonamides. (A) The insertion of rigid polyproline linkers should lead to an increased distance between the two fluorophores in the open state of the sensor protein and thereby also to less FRET. The distance of the two fluorophores in the closed state of the sensor protein should not be significantly affected. Consequently, the maximum ratio change should increase. (B) Emission spectra of SNAP_PP0_CLIP_HCA at a low and a high concentration of benzenesulfonamide (100 pM, black; 10 mM, white). The addition of benzenesulfonamide leads to an increase in the Cy3/Cy5 emission ratio with a maximum ratio change of 1.9 ± 0.1. (C) Emission spectra of SNAP_PP30_CLIP_HCA at a low and a high concentration of benzenesulfonamide (100 pM, black; 10 mM, white). The addition of benzenesulfonamide leads to an increase in the Cy3/Cy5 emission ratio with a maximum ratio change of 4.9 ± 0.3. (D) Fluorescence titration curves of the optimized sensor proteins. Shown is the ratio of fluorescence of donor (570 nm) and acceptor emission (670 nm) obtained by titrating the corresponding labeled sensor mutant with benzenesulfonamide. The data are represented as the mean $\pm$ standard deviation of triplicates. The sensor data are fitted according to a single-site binding isotherm. (E) Bar graph of the measured maximum ratio changes for each sensor mutant. For comparison, the maximum ratio change of the original sensor protein[15] is also displayed. All maximum ratio changes for the different sensor mutants were obtained by dividing the F_{max} value by the F_0 value obtained after fitting the sensor mutant's benzenesulfonamide titration data (Supporting Information). The data are represented as the mean $\pm$ standard deviation of triplicates.

their well-defined property of forming a stable and rigid helical structure (the polyproline II helix) with a pitch of 3.1 Å per residue in aqueous solution.[25−27] We constructed seven sensor mutants in which the peptide linkers between CLIP-tag and HCA were removed, and polyproline linkers of varying length (0, 6, 9, 12, 15, 30, 60) were inserted between SNAP- and CLIP-tag to replace the original peptide linker. According to our model,

this should increase the distance between the fluorophores mainly in the open state of the sensor and should thus result in an increased maximum ratio change (Figure 5A).

All seven sensor mutants could be successfully expressed and purified from *E. coli* (Figure S11). After labeling with BG-PEG$_{11}$-Cy5-SA and with CLIP-Surface 547, the mutants were tested for their ability to sense sulfonamide in vitro. We found that increasing
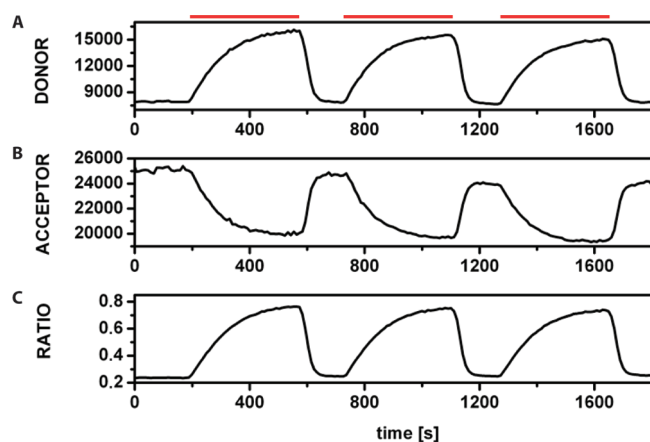
Figure 6. Optimized sensor protein SNAP_PP30_CLIP_HCA on the surface of HEK 293T cells. (A) Time course of the donor channel of the sensor protein SNAP_PP30_CLIP_HCA upon addition and removal of 10 mM benzenesulfonamide. The addition of 10 mM benzenesulfonamide leads to an increased donor emission. (B) Time course of the acceptor channel of the sensor protein SNAP_PP30_CLIP_HCA upon addition and removal of 10 mM benzenesulfonamide. The addition of 10 mM benzenesulfonamide leads to a decreased acceptor emission. (C) Time course of the intensity ratio of donor emission vs acceptor emission upon addition and removal of 10 mM benzenesulfonamide. The red bar indicates the time span of perfusion with benzenesulfonamide.

the length of the polyproline linker between SNAP- and CLIP-tag also increases the maximum ratio change of the sensor mutant increases. The best sensor mutant SNAP_PP60_CLIP_HCA displayed a maximum ratio change of 6.9 ± 0.7 (Figure S12); however, its K_d^{comp} value was lower than those of the other constructs, which showed no significant differences (Figure S13). For all further studies we therefore focused on the mutant SNAP-PP30-CLIP-HCA, which displays a maximum ratio change of 4.9 ± 0.3 (Figure 5). Our findings are in accordance with our optimization predictions and prove that increasing the linker length between SNAP- and CLIP-tag indeed leads to improved sensor mutants. Further, the similar K_d^{comp} values measured for our sensor mutants up to a linker length of 30 prolines indicate that the insertion of these peptide linkers does not significantly change the effective molarity of the intramolecular ligand; i.e., they do not seem to induce an intramolecular aggregation or to hinder sensor closing.

According to the sensor model, decreasing the linker between CLIP-tag and HCA should lead to a shorter distance between the two fluorophores in the closed state and therefore to an optimized sensor mutant. In our polyproline sensor mutants we have already removed the six amino acid linker between CLIP-tag and HCA. A further deletion of amino acids from the N-terminus of HCA results in a reduced stability of the protein.[28,29] Thus, to test our mechanistic predictions, we decided to rather construct a sensor mutant with an increased linker length between CLIP-tag and HCA. According to our optimization guidelines this sensor protein should then display a decreased maximum ratio change compared to the original sensor protein. Insertion of 15 proline residues between CLIP-tag and HCA resulted in sensor protein SNAP_CLIP_PP15_HCA. In accordance with our predictions, we found that the insertion of 15 proline residues between CLIP-tag and HCA almost completely eliminated the signal change of the sensor protein upon addition of benzenesulfonamide (Figure S14).

In a next step, we wanted to test the performance of our two best sensor mutants SNAP_PP15_CLIP_HCA and SNAP_PP30_CLIP_HCA on the cell surface of mammalian cells. Both sensor proteins could be successfully expressed and labeled on the surface of HEK 293T cells. The expression level of the sensor mutants was found to be very similar to the one of the original SNAP_CLIP_HCA sensor protein (Figure S15); thus, the introduction of long polyproline stretches into the sensor protein does not seem to influence the expression and the trafficking of the sensor protein to the cell surface. Upon perfusion with 10 mM benzenesulfonamide, we measured a maximum ratio change of 2.1 ± 0.1 for the sensor protein SNAP_PP15_CLIP_HCA (Figure S16), and a maximum ratio change of 3.3 ± 0.4 for the most optimized sensor protein SNAP_PP30_CLIP_HCA (Figure 6). This signifies a major improvement compared to the original sensor protein (ΔR_{max} of 1.5) and proves that our sensor proteins can be rationally optimized for their application on the cell surface. Further, the ΔR_{max} of our best sensor protein is clearly superior than PBP-based FRET reporters displayed on cell surfaces, which have not yet achieved a ΔR_{max} of more than 1.5.[10]

■ CONCLUSIONS

In summary, we have demonstrated the successful implementation of our Snifit sensor proteins on the surface of mammalian cells. This is an important accomplishment as the adaption of sensors to applications in living cells represents a major challenge in the field. Further, a thorough characterization of the Snifit sensor proteins has been carried out including the description of its thermodynamic and kinetic properties. We have also successfully validated our proposed optimization guidelines thereby proving that it is possible to rationally optimize Snifit sensor proteins. The rational engineering of the peptide linkers of the Snifit sensor protein allowed an improvement of the sensor's dynamic range from 1.8 to 4.9 in vitro. On the cell surface, the maximum ratio change could be improved from 1.5 to 3.3, thereby producing FRET sensor proteins for the cell surface with unprecedented maximum ratio changes.

The use of self-labeling tags instead of FPs for Snifit sensor construction offers several advantages: (i) a large choice of fluorophores with tailor-made properties is available for the construction of the sensor protein starting from a single sensor construct; (ii) the application of membrane-impermeable dyes allows an exclusive labeling of the subpopulation of sensor proteins that are properly trafficked to the cell surface; and (iii) the sensor response rate upon emergence of the metabolite of interest can be tuned by choosing an appropriate intramolecular ligand. Finally, since our sensor concept circumvents the need for a conformational change of the binding protein, the herein presented work provides the necessary basis for the generation of sensor proteins for the detection of previously inaccessible metabolites on the cell surface of mammalian cells.

■ METHODS

Synthesis. Detailed synthetic procedures and characterizations are described in the Supporting Information.

Cell Culture and Transfection. HEK 293T cells were grown on polylysine coated glass coverslips (Ø 15 mm) in DMEM Glutamax medium (Lonza) supplemented with 10% fetal bovine serum (Lonza) and transiently transfected by using Lipofectamine (Invitrogen) according to the manufacturer's protocol.

SNAP- and CLIP-Tag Labeling on the Cell Surface of HEK 293T Cells. Twenty-four hours after transfection, HEK 293T cells were labeled with a solution of 2 μM of the corresponding BG derivative and 10 μM of the corresponding O^2-benzylcytosine (BC) derivative in Hank's buffered salt solution (HBSS) complemented with 10 mg/mL BSA for 10 min at room temperature. After being labeled, cells were washed four times with HBSS.

Confocal Microscopy. Images of HEK 293T cells labeled with CLIP-Surface 547 and with SNAP-Surface 647 were taken using a Zeiss LSM 700 confocal microscope equipped with a 40× plan Apochromat 1.3 numerical aperture (NA) oil immersion objective lens. The imaging was performed using a 555 nm laser line for excitation of DY-547 and a 639 nm laser line for excitation of DY-647. Fluorescence was collected at 400−620 nm and at 620−700 nm for DY-547 and DY-647, respectively. The settings for scanning were: ×2 zoom, image format 1024 × 1024 pixels, pinhole 1Airy unit (AU), average 16 frames.

Wide-Field Microscopy and Live Cell FRET Imaging. Glass coverslips with labeled HEK 293T cells were transferred to a Warner imaging chamber (RC-20). Perfusion of the chamber was performed gravity-fed at a flow rate of 0.5 mL/min. Time-course experiments of sensor imaging were performed using a Leica LAS AF 7000 wide-field microscope equipped with a 40× plan Apochromat 1.25 NA oil immersion objective lens. A xenon arc lamp was used for imaging of the HEK 293T cells. For each frame, the two channels (donor and FRET) were measured consecutively with an interval of 30 ms between the two emission channels. The following filter sets were used for the FRET ratio imaging: for DY-547/Cy5, excitation at 530 nm (bandwidth 35 nm), emission at 580 nm (bandwidth 40 nm) (DY-547) and at 700 nm (bandwidth 72 nm) (Cy5); for Alexa Fluor 488/DY-547, excitation at 470 nm (bandwidth 40 nm), emission at 520 nm (bandwidth 40 nm) (Alexa Fluor 488) and at 605 (bandwidth 70 nm) (DY-547); for Alexa Fluor 488/Alexa Fluor 594, excitation at 470 (bandwidth 40 nm), emission at 520 nm (bandwidth 40 nm) (Alexa Fluor 488) and at 632 nm (bandwidth 60 nm) (Alexa Fluor 594). If not indicated otherwise, the image size was 293 μM × 293 μM, and an average of 5 cells per image were analyzed for the intensity ratio plots.

ASSOCIATED CONTENT

Ⓢ Supporting Information. Synthetic procedures, characterizations of the sensor proteins on the cell surface and in vitro, and complete ref 1. Additional figures and tables. This material is available free of charge via the Internet at http://pubs.acs.org.

AUTHOR INFORMATION

Corresponding Author
kai.johnsson@epfl.ch

Present Addresses
†Department of Chemistry, National Tsing Hua University, Hsinchu 30013, Taiwan.
‡Institute for Molecules and Materials, Department of Organic Chemistry, Radboud University Nijmegen, 6525 AJ Nijmegen, The Netherlands.

ACKNOWLEDGMENT

REFERENCES

(1) Wishart, D. S.;; et al. *Nucleic Acids Res.* **2009**, *37*, D603–D610.
(2) Sassone-Corsi, P.; Nakahata, Y.; Sahar, S.; Astarita, G.; Kaluzova, M. *Science* **2009**, *324* (5927), 654–657.
(3) Zhang, J.; Newman, R. H.; Fosbrink, M. D. *Chem. Rev.* **2011**, *111* (5), 3614–3666.
(4) Breaker, R. R. *Nature* **2004**, *432* (7019), 838–845.
(5) Navani, N. K.; Li, Y. F. *Curr. Opin. Chem. Biol.* **2006**, *10* (3), 272–281.
(6) Ibraheem, A.; Campbell, R. E. *Curr. Opin. Chem. Biol.* **2010**, *14* (1), 30–36.
(7) Wiechert, W.; Schweissgut, O.; Takanaga, H.; Frommer, W. *Curr. Opin. Plant Biol.* **2007**, *10* (3), 323–330.
(8) Okumoto, S. *Curr. Opin. Biotechnol.* **2010**, *21* (1), 45–54.
(9) Fehr, M.; Takanaga, H.; Ehrhardt, D.; Frommer, W. *Mol. Cell. Biol.* **2005**, *25* (24), 11102–11112.
(10) Hires, S.; Zhu, Y.; Tsien, R. *Proc. Natl. Acad. Sci. U.S.A.* **2008**, *105* (11), 4411–4416.
(11) Lager, I.; Looger, L.; Hilpert, M.; Lalonde, S.; Frommer, W. *J. Biol. Chem.* **2006**, *281* (41), 30875–30883.
(12) Okumoto, S.; Looger, L.; Micheva, K.; Reimer, R.; Smith, S.; Frommer, W. *Proc. Natl. Acad. Sci. U.S.A.* **2005**, *102* (24), 8740–8745.
(13) Medintz, I. *Trends Biotechnol.* **2006**, *24* (12), 539–542.
(14) Deuschle, K.; Fehr, M.; Hilpert, M.; Lager, I.; Lalonde, S.; Looger, L.; Okumoto, S.; Persson, J.; Schmidt, A.; Frommer, W. *Cytometry, Part A* **2005**, *64A* (1), 3–9.
(15) Brun, M. A.; Tan, K. T.; Nakata, E.; Hinner, M. J.; Johnsson, K. *J. Am. Chem. Soc.* **2009**, *131* (16), 5873–5884.
(16) Keppler, A.; Gendreizig, S.; Gronemeyer, T.; Pick, H.; Vogel, H.; Johnsson, K. *Nat. Biotechnol.* **2003**, *21* (1), 86–89.
(17) Keppler, A.; Arrivoli, C.; Sironi, L.; Ellenberg, J. *Biotechniques* **2006**, *41*, (2), 167.
(18) Lavis, L.; Raines, R. *ACS Chem. Biol.* **2008**, *3* (3), 142–155.
(19) Krishnamurthy, V. M.; Kaufman, G. K.; Urbach, A. R.; Gitlin, I.; Gudiksen, K. L.; Weibel, D. B.; Whitesides, G. M. *Chem. Rev.* **2008**, *108* (3), 946–1051.
(20) Campbell, R. E. *Anal. Chem.* **2009**, *81* (15), 5972–5979.
(21) Nguyen, A. W.; Daugherty, P. S. *Nat. Biotechnol.* **2005**, *23* (3), 355–360.
(22) Ouyang, M. X.; Sun, J.; Chien, S.; Wang, Y. X. *Proc. Natl. Acad. Sci. U.S.A.* **2008**, *105* (38), 14353–14358.
(23) Golynskiy, M. V.; Rurup, W. F.; Merkx, M. *ChemBioChem* **2010**, *11* (16), 2264–2267.
(24) Evers, T.; van Dongen, E.; Faesen, A.; Meijer, E.; Merkx, M. *Biochemistry* **2006**, *45* (44), 13183–13192.
(25) Arora, P. S.; Ansari, A. Z.; Best, T. P.; Ptashne, M.; Dervan, P. B. *J. Am. Chem. Soc.* **2002**, *124* (44), 13067–13071.
(26) Stryer, L.; Haugland, R. P. *Proc. Natl. Acad. Sci. U.S.A.* **1967**, *58*, (2), 719.
(27) Schuler, B.; Lipman, E. A.; Steinbach, P. J.; Kumke, M.; Eaton, W. A. *Proc. Natl. Acad. Sci. U.S.A.* **2005**, *102* (8), 2754–2759.
(28) Aronsson, G.; Martensson, L. G.; Carlsson, U.; Jonsson, B. H. *Biochemistry* **1995**, *34* (7), 2153–2162.
(29) Vince, J. W.; Carlsson, U.; Reithmeier, R. A. F. *Biochemistry* **2000**, *39* (44), 13344–13349.